Chapter-6

Fabrication and Electrical characterization of GO/PMMA, rGO-ZnO/PMMA based flexible resistive memory devices.

6.1 Device Fabrication

Polymethyl methacrylate was dissolved in Dimethyl formamide at a concentration of 30 mg/ml. The solution was kept on a magnetic stirrer overnight to allow complete dissolution. Separately, GO nanosheets and rGO-ZnO heterostructures were dispersed in DMF via ultrasonication to break down any agglomerates and exfoliate the nanosheets. The two solutions were then mixed and ultrasonicated for 6 hrs to allow successful grafting of nanosheets/heterostructures on the polymer chains to prepare a highly homogenous precursor solution with absence of phase separation. The weight fraction of GO nanosheets/ rGO-ZnO heterostructures in PMMA was kept at 0.5 wt%. Prior to spin coating, the PET-ITO substrates were thoroughly treated to remove any impurities and obtain a homogenous surface. The typical process consisted of sequential sonication for 10 min each in DI water, acetone and isopropyl alcohol. Finally, the surface was plasma treated (Diener plasma surface technology) for 10 min under 0.5 mbar pressure and 20-watt excitation power to increase the adhesion with polymer chains. The nanocomposite precursor solution was spin coated at a speed of 1500rpm for 60 s using Spin NXG-P2 spin coating system by Apex instruments. The spin-coated layer was annealed in a vacuum oven at 70ºC for 1 hour to facilitate the evaporation of residual solvent. The device structure was completed with the deposition of top Al electrodes (100 nm thickness) using the thermal evaporation technique. The schematic representation of M1 device structure is presented in Fig 6.1. The thickness of the active switching layer of the devices was measured using AFM and the results are presented in Fig 6.2.

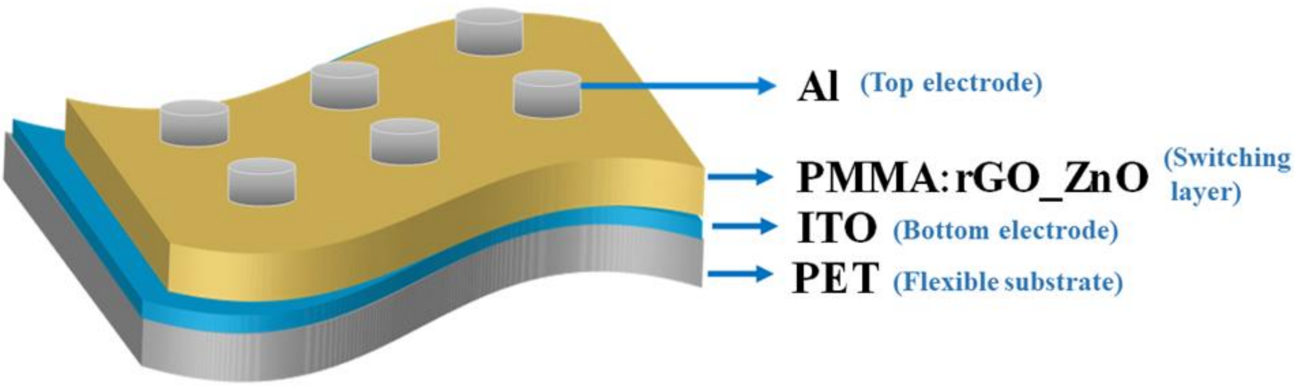

Fig 6.1: Schematic of hierarchical architecture of hybrid heterostructure based flexible device.

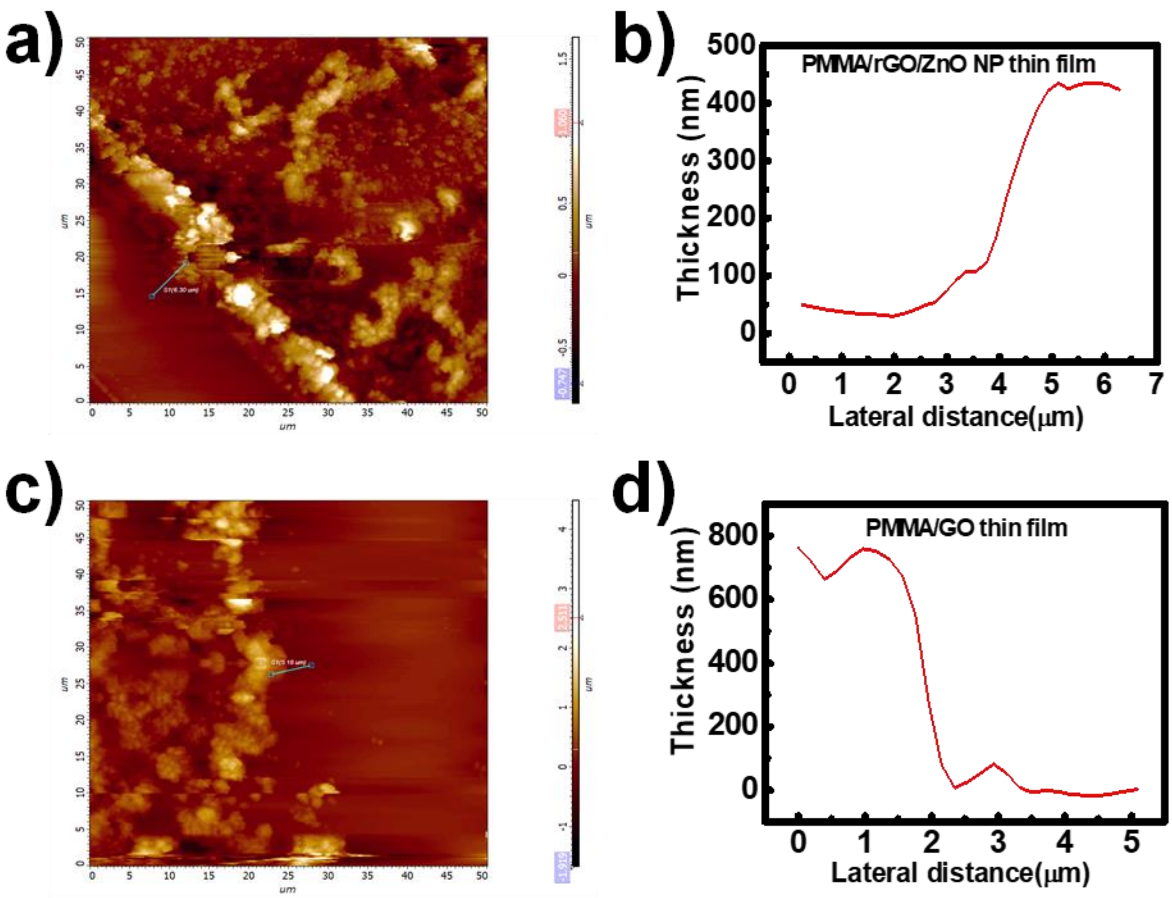

Fig 6.2: AFM picture in the scratched area of PNC film a) PMMA/rGO/ZnO film and c) PMMA/GO film. Line scan height profile of b) PMMA/rGO/ZnO film and, d) PMMA/GO film

6.2 Electrical characterization of devices

Bistable resistive switching behavior was studied for the two fabricated devices- 1) PET/ITO/PMMA-GO/Al (denoted as M2) and 2) PET/ITO/PMMA-rGO_ZnO/Al (denoted as M1). The M2 device with PMMA encapsulated GO nanosheets has been used as a reference architecture to compare and analyze the enhanced performance bestowed by hybrid rGO-ZnO heterostructure based device. The electrical characterization consisted of cyclic I-V measurements, endurance and retention characteristics. B1500 semiconductor characterization system manufactured by Keysight technologies was utilized for this purpose. Conduction mechanism of the M1 device was investigated using the double logarithmic I-V plots. Energy band gap modelling of the M1 device was conducted to illuminate the carrier mechanism. Rigorous flexibility studies were carried out on an in-house designed bending apparatus.

Flexibility data was utilized to deduce the bending endurance and critical bending radius of the M1 device.

6.3 Results & Discussion

6.3.1 Electrical characterization

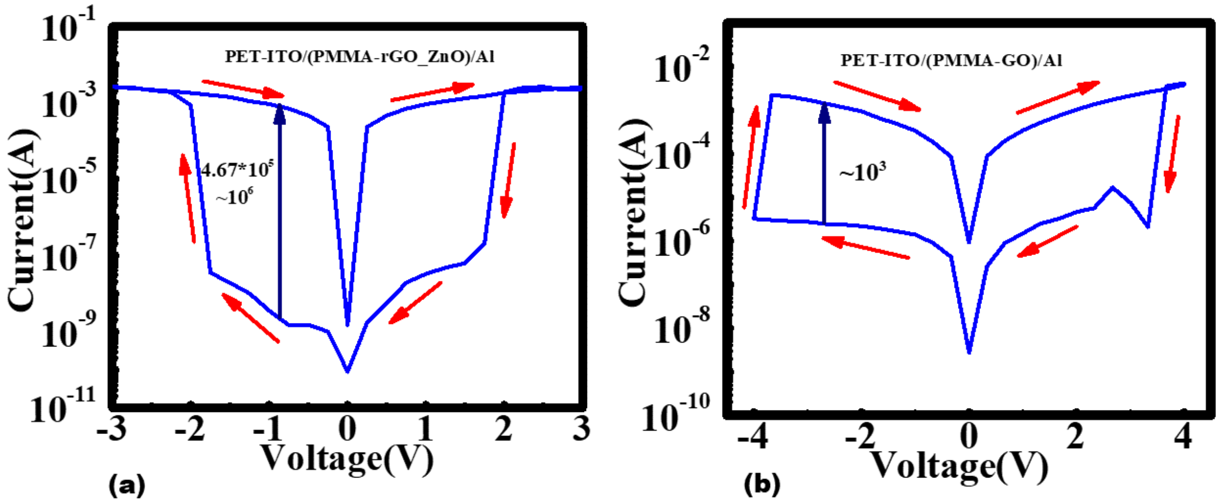

Fig 6.3: I-V characteristics of a) M1 device and b) M2 device depicting bistable non-volatile memory operation.

Bistable memory operation

Fig 6.3 b displays the I-V characteristics of the M2 device. The switching measurements were performed for a voltage sweep from -4V to +4 V at room temperature (27ºC). The compliance current value was fixed at 10 mA to prevent permanent breakdown of the device. For the forward sweep cycle 0 to -4V, the device remained in the high resistance (OFF) state for voltages less than the Vset value. At V_{set} value of -3.8V an abrupt increase in the injection current was observed and the device switched from the HRS(OFF) state to the LRS(ON) state. This is referred to as the SET process and is equivalent to the data writing operation. The device remained in the LRS (ON) state even after removal of the applied bias and further application of the opposite polarity bias 0 to +4V. This demonstrated the storage operation or the non-volatile memory behavior of the device. During the voltage sweep 0 to +4V, a sudden decrease in the injection current was observed at +3.67V and the device switched from the LRS(ON) state to the HRS(OFF) state. This is referred to as the RESET operation and is equivalent to the data erasing operation. To again achieve the ON state, reverse voltage sweep from +4V to -4V was applied. The device retained its OFF state until a voltage of -3.8 (Vset) was reached and again switched back to its ON state thus establishing the rewrite operation. The current ratio between the LRS state and HRS state I_{ON}/I_{OFF} was measured to be of the order of ~10^3.

Fig 6.3a displays the I-V characteristics of the M1 device. The switching measurements were performed for a voltage sweep from -3V to +3V at room temperature (27ºC). The compliance current value was kept same as the M1 device (10mA). The device was initially in the HRS (OFF) state and switched to the ON state in the forward voltage sweep from 0 to -3V at a V_{set} value of -1.7V (write operation). The device retained its ON state even after removal of the applied bias and application of opposite polarity (data storage operation). An abrupt decrease in the injection current was observed during the voltage sweep 0 to +3V at a V_{reset} value of +1.98 V and the device switched to the HRS (OFF) state which represents the data erase operation or the RESET process. The device again switched back to the ON state on application of V_{set} -1.7V during the reverse voltage sweep +3V TO -3V thus successfully establishing the rewritable memory operation. (WRITE-READ-ERASE-READ-REWRITE). It is imperative to note that the introduction of hybrid rGO_ZnO heterostructures in the PMMA matrix significantly decreased the operating voltages of the M1 device as compared to the reference M2 device. V_{set} value observed a shift from -3.8 to -1.7V while the V_{reset} value was decreased from +3.67V to +1.98V. The current value in the high resistance state of the M1 device was also extremely low ($2.14*10^{-9}$ A) which contributed to a radically enhanced I_{ON}/I_{OFF} ratio of the order of ~10^6 which is 1000 times larger than the GO-PMMA nanocomposite layer based memory device.

This significant enhancement in the M1 device performance is attributed to multiple factors- (a) Transformation of GO to rGO improves the stability and conductivity of the nanosheets through the removal of oxygen containing functional groups from the GO surface. (b) High electron mobility, wide band gap and rich oxygen vacancy concentration of ZnO nanostructures radically enhances the charge trapping and transport capabilities of the active layer. (c) Formation of interfacial energy barriers and p-n heterojunctions inside the in situ grown rGO-ZnO heterostructures further contributes to the improved electrical performance. The low operating voltages can significantly reduce the power consumption of the device which is one of the most important factors for application in next generation miniature flexible and portable electronic systems. Additionally, a remarkably high separation (order of ~10^6) between the OFF and ON state could dramatically enhance the reliability of the read and write operations thus establishing our polymer encapsulated hybrid 2D-3D heterostructure based memory device as an excellent candidate for flexible electronics such as IoT devices, bendable electronics, portable miniaturized devices, wearable sensors, etc.

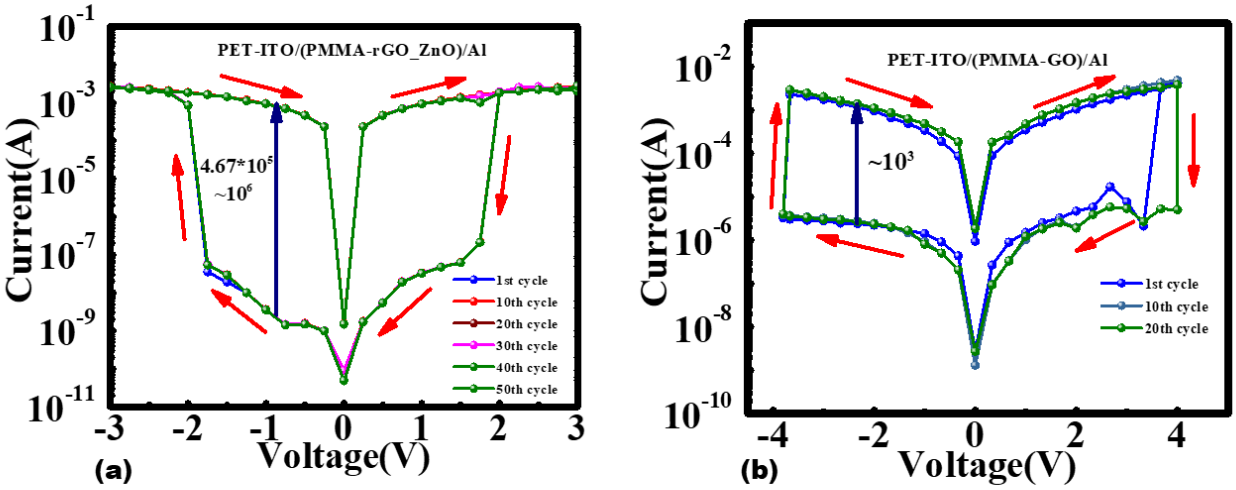

Fig 6.4: Endurance cycle measurements of a) M1 device and b) M2 device

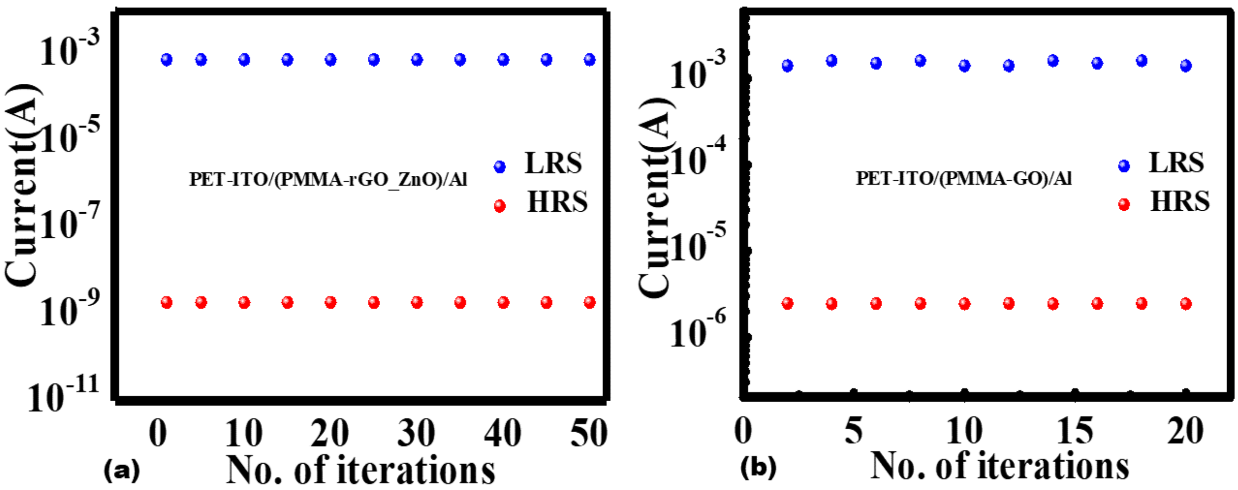

Fig 6.5: Current values in HRS and LRS after multiple switching cycles for a) M1 device and b) M2 device

6.3.2 Endurance and Retention characteristics

Endurance analysis involves measuring the number of switching cycles that the device can withstand before experiencing a significant degradation in performance. Fig 6.4-a and b depicts the I-V characteristics of the M1 device (PET/ITO/PMMA-rGO_ZnO/Al) and M2 device (PET/ITO/PMMA-GO/Al) respectively for multiple iterations. It was observed that the M2 device displayed stable performance for just 20 cycles while the heterostructure based M1 device exhibited negligible degradation for over 50 cycles. The current value in the HRS and LRS was measured after a fixed number of cycles to demonstrate the stable operation of the devices and is presented in Fig 6.5.

Retention analysis involves measuring the amount of time that the device can retain its state (either LRS or HRS) after the applied voltage is removed. Initially, a set voltage was applied to the device which was then removed and the current values in the HRS and LRS were recorded at an interval of 60s. Retention behavior of the M1 and M2 device is depicted in fig 6.6-a and b respectively. The LRS (ON) state of the M2 device suffered serious degradation after a period of 10^3s while the HRS (OFF state) remained stable for 10^3s. The M1 device, as expected, displayed excellent retention characteristics with the LRS exhibiting stable retention for a period of 10^4s while the HRS experienced slight degradation post $3*10^3$s.

M2 device with GO/PMMA as the active layer exhibited lower endurance and retention performance compared to M1 device with rGO_ZnO/PMMA as the active layer. This was attributed to the fact that the oxygen-containing functional groups in GO can degrade over time due to exposure to heat and electrical stress while the rGO nanosheets due to absence of structural defects and decreased oxygen-containing functional groups exhibit enhanced stability. Additionally, the formation of p-n heterojunctions in the rGO_ZnO heterostructures further enhances the interfacial interactions and contributes to increased cycling and retention stability.

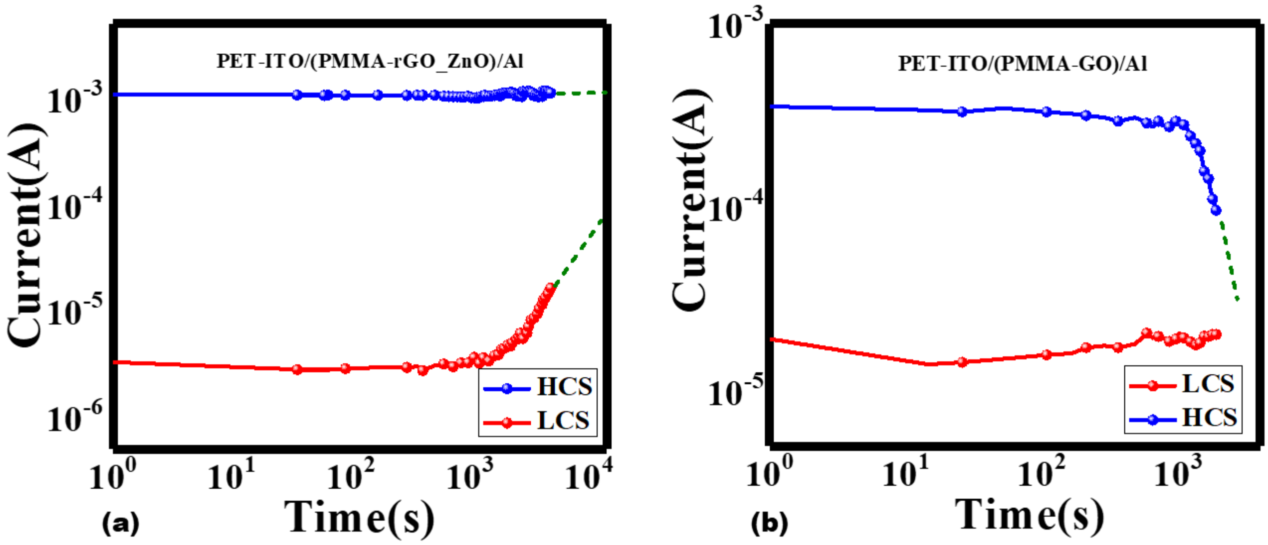

Fig 6.6: Retention time measurements of high conductance state (HCS) and low conductance state (LCS) of a) M1 device and b) M2 device

6.3.3 Flexibility study

The device was fabricated using flexible PET substrate for potential application in next generation flexible and wearable electronics. For practical device applications, mechanical and electrical stability under repeated bending operations is a necessary requirement. In order to evaluate the flexibility performance of the M1 device, I-V characteristics were recorded for the flat configuration and under various bending stresses using an in-house bending setup. The digital image of the fabricated flexible device and the bending apparatus is presented in Fig 6.8(inset). Fig 6.7 displays the I-V characteristics under a bending radius of 10mm, 8mm and an extreme bending radii of 6mm and 4mm. It could be observed that the device exhibited excellent electrical performance even under a critical bending radii of 6mm. The I_{ON}/I_{OFF} ratio was measured to be ~ 10^6 and the operating voltages also remained under -3V/+3V. On further bending beyond the critical radius of 6mm, the device suffered drastic degradation owing to the mechanical damage of the active layer and disintegration of the electrodes. This was inferred from the I_{ON}/I_{OFF} ratio which significantly decreased by more than 10^4 orders of magnitude and the threshold voltage shifted beyond the operating range of -4V. The current values of HRS and LRS in the flat configuration and under various bending radii are presented in Fig 6.8 b.

The flexibility performance was further analyzed by studying the bending endurance of the device. A fixed value of bending radius (10mm) was utilized for this experiment. The current values in the HRS and LRS were recorded after every 100 bending cycles to demonstrate the electrical stability of the flexible device under repeated mechanical stress. Results of the bending endurance of M1 device are presented in Fig 6.8 a. It could be observed from the HRS and LRS current values that the device exhibited extremely stable electrical characteristics even after 1000 continuous bending cycles thus successfully establishing its practical applicability in flexible and portable electronics.

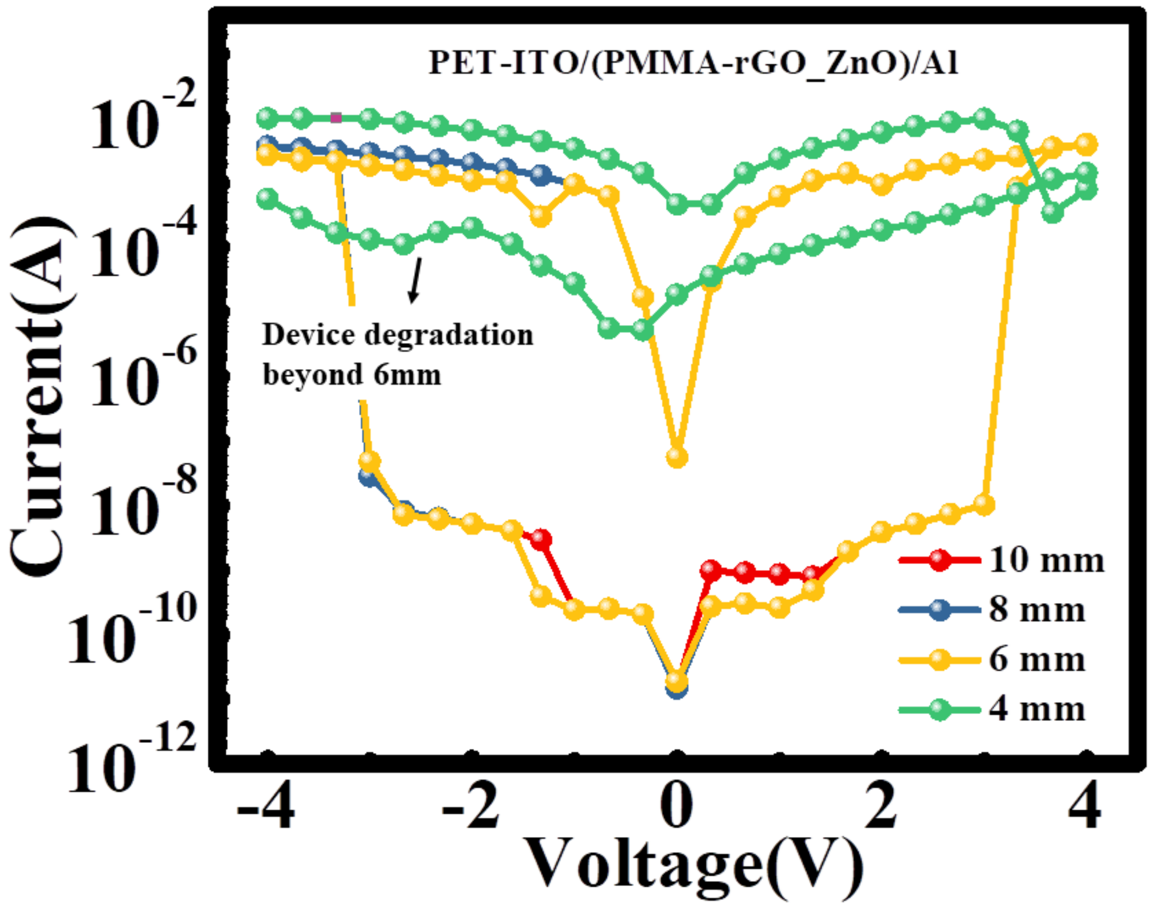

Fig 6.7: I-V characteristics of M1 device under different bending radii.

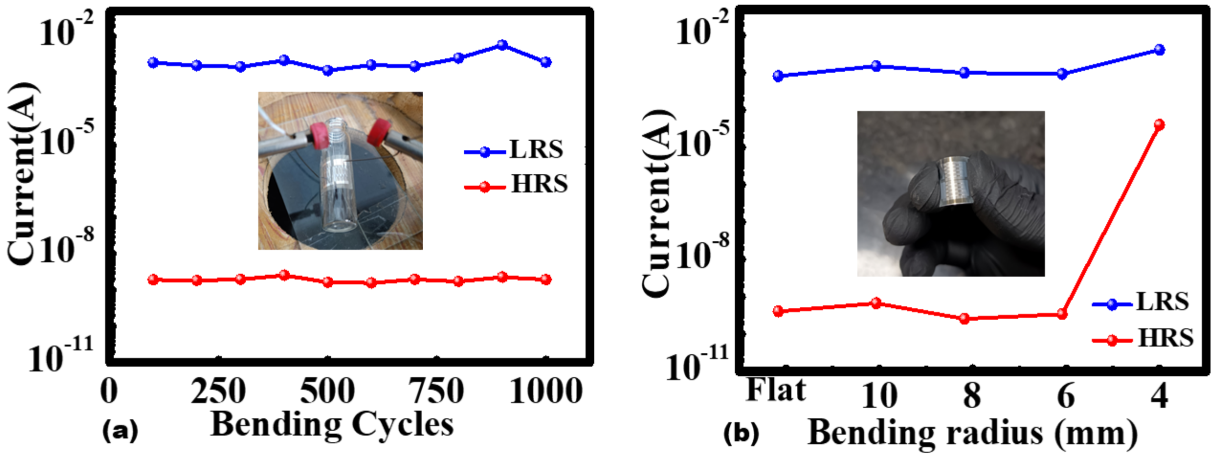

Fig 6.8: a) Current values of M1 device in the HRS and LRS after multiple bending cycles, b) Current values of M1 device in the HRS and LRS under different bending radii and without bending.

6.3.4 Band-gap modelling and carrier mechanism

This reversible switching behavior of M1 can be realized through external bias dependent band bending, charge carrier accumulation/removal in rGO/ZnO NP and subsequent transport to the electrode. Fig 6.9 a) presents the energy band diagram of the hierarchical device architecture of M1 device (PET/ITO/(PMMA-rGO/ZnO NP)/Al) in HRS without any external bias. The zoom view of energy band diagram of PMMA-rGO/ZnO NP is shown in Fig 6.9 b). When negative voltage is applied to the Al electrode, electrons are injected to the LUMO level of rGO/ZnO NP through PMMA layer via Fowler-Nordheim tunneling (FN). [187] Owing to the significantly higher electron affinity of rGO/ZnO NP (4.75 eV) [188] compared to the LUMO level of PMMA (1.65 eV), the rGO/ZnO NP layer acts as an electron trapping and transport layer. Additionally, ZnO also has a higher electron affinity (4.3 eV) [189] and a wide band gap of 3.2 eV (derived from UV-Vis absorption data) which further enhances the charge-trapping capabilities of the active layer. PMMA also plays the role of hole blocking layer and prevents the migration of holes from ITO to the active layer due to a larger energy gap between the work function of ITO (4.8 eV) and HOMO level of PMMA (7.25 eV) [190]. Besides, the larger band gap of PMMA (5.6 eV) prevents the carrier recombination in the active layer and aids the accumulation of electrons at the charge trapping centers (Fig 6.9 c).

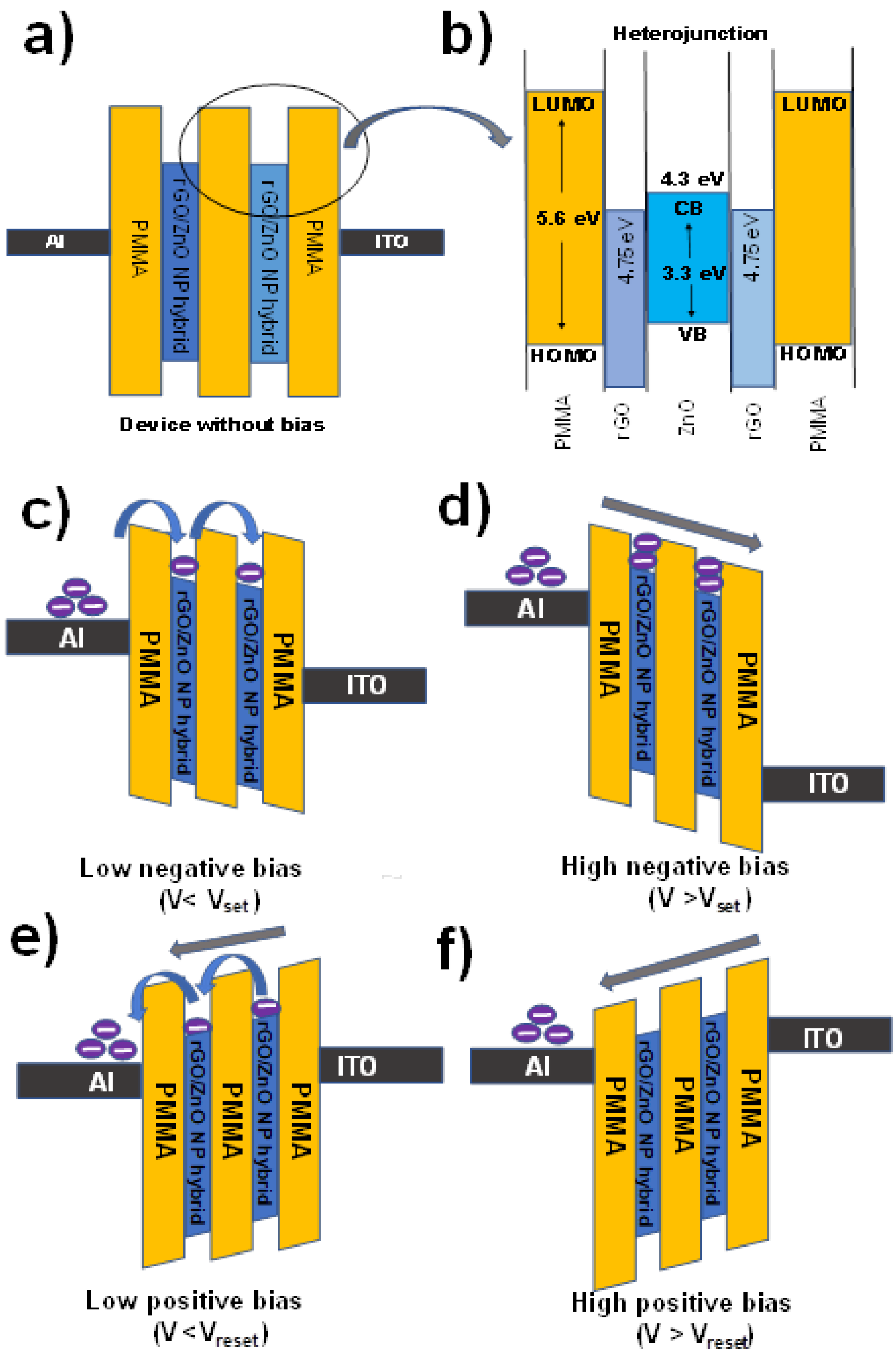

Fig 6.9: Band-gap modelling of M1 device depicting the carrier mechanism; a) Energy band without bias, b) zoom view of PMMA/(rGO/ZnO NP)/PMMA, c) device under low negative bias, d) device under high negative bias, e) device under low positive bias, f) device under high positive bias.

Although this charge trapping phenomena continues up to the time of maximum capability of the rGO/ZnO NP layer. Further increase in external bias saturates that capacity and subsequently results in the formation of a conductive pathway between the top Al and bottom ITO electrode, referred to as the conducting filament. The formation of a dense conductive filament switches the device from the HRS/OFF state to the LRS/ON state through space-charge-limited current (SCLC) mechanism. This is representative of the SET operation or Writing process (Fig 6.9 d). The PMMA/(rGO/ZnO NP)/PMMA network retains the trapped electrons even after removing the applied bias resulting in the storage operation. Besides, if a positive voltage sweep is applied, initially, the LRS/ON state is retained up to a certain external bias ($V < V_{reset}$) (Fig 6.9 e). During this step, trapped electrons are slowly removed by maintaining its' LRS/ON state. However, the device switches from the LRS to HRS only after applying a sufficient positive bias which removes most of the trapped electrons from the rGO/ZnO NP layer. By this way, on application of positive V_{reset} the electrons are detrapped and revert to the top Al electrode again via FN tunneling process and the device switches back to the HRS/OFF state. (Fig 6.9 f). This trap-controlled SCLC mechanism and FN tunneling continues in cyclic ways to provide such unique non-volatile bistable memory characteristics to the rGO/ZnO NP heterostructure based device.

6.3.5 Conduction Mechanism

I-V characteristics of the M1 device were plotted in double logarithmic scale to elucidate the conduction mechanism of the device in LRS and HRS. (Fig 6.10**)** The LRS or ON state displays an ohmic behaviour with I showing a linear relationship with applied bias and possesses a slope $\alpha 1\sim 1.02$. Owing to the formation of a conductive pathway between the top and bottom electrode, assisted by the FN tunneling process, the device behaves like an ohmic conductor. The HRS or OFF state consists of three different regions. Region 1 depicts ohmic conduction at low applied voltage since the low applied bias is insufficient to cause the detrapping of electrons from the charge trapping centers and hence the current varies linearly with V with a slope value $\alpha 1\sim 1.17$. Region 2 accurately obeys the Mott gurney law for semiconductors according to which free charged particles in a semiconducting medium drift with a specific velocity $v=\mu e$ and the current density is proportional to the square of applied bias, $I \sim V^2$. The slope calculated from the ln-ln I-V characteristics in region 2 came out to be in excellent agreement with $\alpha 2\sim 2.07$. Region 3 depicts a steep increase in the current value

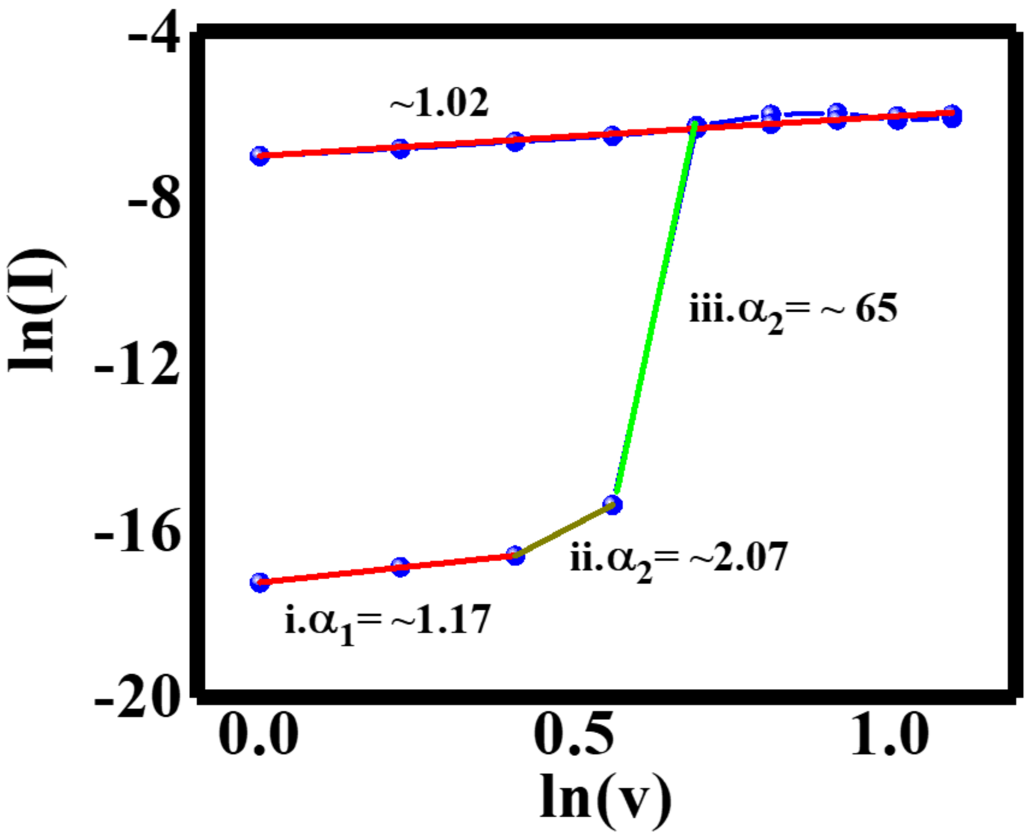

Fig 6.10: I-V characteristics of M1 device in double logarithmic scale illuminating the conduction mechanism in both HRS and LRS.

compared to a small change in the applied bias. The current obeys the relation $I = V^{\alpha}$ where α is an integer, usually greater than 4 for trap controlled SCLS mechanism. [191] The slope calculated from region 3 denoted a very high value of α3 ~ 65. Such remarkably high values of α3 are an indication of very strong trap controlled SCLC mechanism.

6.3.6 Electrical and flexibility performance compared to recently reported PNC devices

Overall device performance of this memristor has several good aspects with respect to recent publications of similar PNC based memristors which are listed in Table-1. Out of them high On/Off ratio and bending endurance are two key features. Besides, this device can maintain its

Sr. No.	Device Structure	Current ratio	Bending radius	Bending endurance (cycles)	Reference
1	Al/ZnO– PVA/PEDOT:PSS/Al/ PET	10^5	60^o	Single cycle	[133]
2	Cu/g-MoS2_PMMA/ITO/PET	10^4	10 mm	100 cycles	[131]
3	AgNW/CAQD-PVP/AgNW/ PVP	10^3	15 mm	100 cycles	[192]
4	Ag/Ti3C2Tx/PVA/ITO/PET	<10	5 mm	100 cycles	[193]
5	Ag/Bi2Se3@PMMA/ITO/PET	10^3	10 mm	Single cycle	[194]
6	Ag/Au− chitosan/Au/PET	>10	5 mm	800 cycles	[195]
7	W/egg albumen/ITO/PET	10^2	7 mm	1000 cycles	[196]
8	**Al//(PMMA-rGO/ZnO NP)/ITO/ PET**	$\mathbf{10^6}$	**6 mm**	**1000 cycles**	**This work**

Table 6.1: Flexibility and electrical performance of this device in comparison to recently published literatures.

On/Off ratio in the same order up to the bending radii 6 mm which implies its high allowed mechanical flexibility.

6.4 Conclusion

Highly flexible, non-volatile resistive switching-based memory devices with a hierarchical thin-film architecture were fabricated using low-temperature, cost-efficient solution processing technique. The device structure consists of an ITO-coated flexible PET substrate as the bottom electrode and PMMA-embedded reduced-graphene/ZnO nanoparticle (NP) (rGO/ZnO NP) heterostructure as the flexible active layer. Besides, a rGO/PMMA-based device was also fabricated as reference. The operating voltage of this device is limited within ±2 V whereas the

ON-to-OFF state is ~10^6 which is ~10^3 times higher than the reference device. The device also exhibited excellent endurance and retention characteristics with no significant degradation for more than 50 cycles. Besides, the retention time of this device is ~10^4 s which is several times more than the reference device. These electrical performance enhancements were attributed to the multifunctionality introduced by the rGO/ZnO NP heterostructures. A model based on the energy band of the components of this composite material has been proposed for better understanding of this mechanism. Flexibility studies exhibited a stable device performance for an extreme bending radius of 6 mm. The resistance of the device in ON-to-OFF states did not show any significant change even after 1000 bending cycles thus establishing the device as an excellent memory candidate for flexible and portable electronics.